Geometry-induced fluctuations in the transitionally rough regime

Geometry-induced fluctuations in the transitionally rough regime

Nabil Abderrahaman-Elena and Ricardo García-Mayoral
Engineering Dept. University of Cambridge. Trumpington Street. CB2 1PZ. UK
E-mail: r.gmayoral@eng.cam.ac.uk

Abstract. Direct numerical simulations of turbulent flows over rough surfaces are conducted to investigate the physics of the transitionally rough regime. Different roughness sizes are analysed within the transitional regime, while keeping the shape of the surface geometry constant. To study the effect of roughness on the flow field, a novel decomposition is used to divide the velocity into two components: a turbulent, geometry-independent contribution, and a geometry-induced contribution, whose intensity is modulated by the overlying turbulence. In the onset of the transitionally rough regime, the turbulent component remains essentially unmodified, and it is anticipated that all the roughness effects can be attributed entirely to the geometry-induced fluctuations. As the roughness size increases further, the turbulent component is also modified, and the fluid-surface interaction becomes more complex.

1. Introduction

Turbulent flows over rough surfaces have been studied by engineers and physicists for several decades due to their ubiquity. In industrial applications, roughness usually has an undesirable impact as it generates additional mixing near the wall, which results in an increase of drag. In other applications, however, this additional mixing can be beneficial, for instance to enhance heat transfer. Engineers like Darcy (1857), especially concerned about pressure losses in pipe flows, began studying turbulent flow over rough walls more than a century and a half ago. Since then, there has been a growing interest in rough-wall turbulence, with a large number of experimental, theoretical and numerical works being carried out. Extensive reviews of the subject can be found in Raupach et al. (1991); Jiménez (2004) and Flack and Schultz (2010).

The three regimes in which wall-bounded flows are traditionally classified are sketched in figure 1. For low Reynolds number, the flow is laminar but, as the Reynolds number increases beyond a certain critical value, the flow becomes turbulent. Provided that the characteristic size of roughness is still too small to affect the flow, rough surfaces behave as smooth walls, in what is known as the hydraulically smooth regime. However, for a fixed geometry of characteristic size k, as the Reynolds number increases the value of k^+ increases, where the superscript '+' denotes scaling in wall-units. For a sufficiently large Reynolds number, the roughness begins to affect the turbulent flow as k^+ is no longer negligible. Eventually, k^+ is large and inertial terms dominate even in the roughness sublayer, which is the region in which turbulent fluctuations depend predominantly on the roughness geometry (Schultz and Flack, 2007). The pressure drag is then dominant and the friction becomes independent of viscosity. The friction coefficient reaches an asymptotic state in which it becomes independent of the Reynolds number, as shown

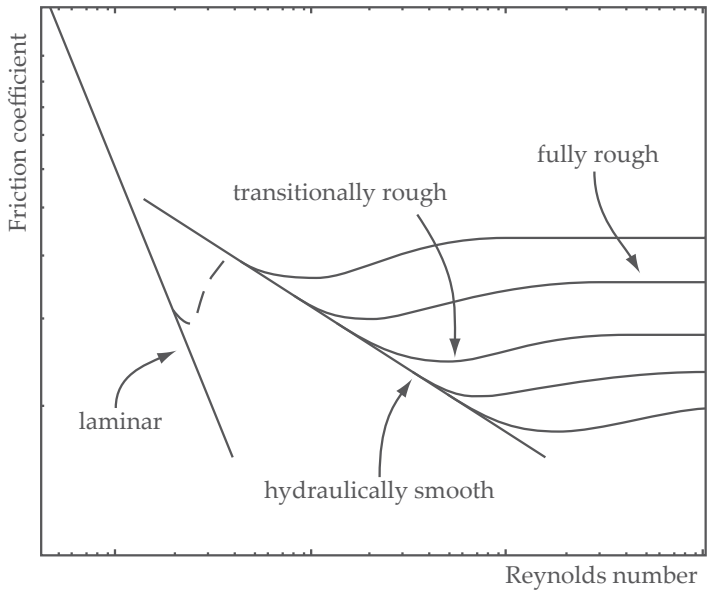

Figure 1. Friction coefficient against bulk-velocity Reynolds number.

in figure 1. This is known as the fully rough turbulent regime. For values of k^+ between the hydraulically smooth and the fully rough regimes, the flow is said to be transitionally rough.

Because of the complexity of any real rough geometry, it is useful to find a simple way to characterise roughness. Nikuradse (1933) conducted a series of experiments in pipe flows with rough walls where the inner walls were coated with packed sand grains of equal size, and measurements were taken for several sand grain sizes. The parameter chosen to characterise the different cases was the sand grain mean diameter, k_s. Far from the wall, Hama (1954) found that roughness only modifies the mean velocity profile by a shift ΔU^+. In the logarithmic region, the shape of the profile and Kármán constant, κ, are otherwise unaffected,

$$U^+(y^+) = \kappa^{-1} \log y^+ + 5.1 - \Delta U^+. \tag{1}$$

Schlichting (1936) found that k_s^+ could be use to characterise any flow over roughness. The strategy is then not to consider the actual roughness size, k^+, but instead to find the equivalent sand grain roughness, k_s^+, which gives the same ΔU^+ as the actual roughness. Any flow with an equivalent sand roughness of k_s^+ produces the same ΔU^+ as a sand roughness of grain size k_s^+. In the fully rough regime, k_s^+/k^+ becomes constant and is only a function of the geometry. However, in the transitionally rough regime k_s^+/k^+ is variable and depends on the flow also. An alternative parameter is $k_{s_\infty}^+$, which is equal to k_s^+ in the fully rough regime, but maintains a constant ratio $k_{s_\infty}^+/k^+$ even in the transitional regime (Jiménez, 2004). As a result, the ratio $k_{s_\infty}^+/k^+$ depends only on the geometry in all the regimes, but different geometries exhibit a different ΔU^+ for the same $k_{s_\infty}^+$ in the transitional regime. Still, ΔU^+ curves eventually collapse in the fully rough regime, as illustrated in figure 3(b).

Starting from $k^+ \approx 0$, as k^+ increases roughness begins to affect the viscous sublayer, friction deviates from hydraulically smooth values, and the flow enters the transitionally rough regime. Some experimental works pay special attention to this regime (Flack et al., 2012; Flack and Schultz, 2014). However the key questions remain unsolved: what mechanism triggers the departure from the hydraulically smooth regime as k^+ increases; and how to define a threshold for this transition based on the roughness geometry only. One of the main issues is that, while $k_{s_\infty}^+$ characterises appropriately the fully rough regime for most rough surfaces, it seems not to be

the correct parameter in the transitionally rough regime. This was already noticed by Colebrook (1939) as his results and Nikuradse's do not match in the mentioned transitional regime. In general, different geometries of roughness lead to different transitions. Comparing several sizes and combinations of sand grains, Colebrook and White (1937) proposed this transition is abrupt in organised geometries, while the presence of a wider range of roughness sizes makes the transition smoother. This assumption is also supported by more recent experiments, such as those using uniformly arranged spherical rough elements by Ligrani and Moffat (1986), in which the transition takes place for even higher values of $k^+_{s_\infty}$, compared to Nikuradse's and Colebrook's experiments, but also in a sharper manner. What is more, the discrepancy is such that Flack and Schultz (2010) report a relatively wide range of experimental values in which the transition takes place, spanning between $1.4\text{–}15 < k^+_s < 18\text{–}70$.

Recent research by Chung et al. (2015) is aiming to find a methodology to capture the effect of roughness, particularly the increase in friction and ΔU^+, at a minimum cost. They conduct fully turbulent simulations, but in minimal-span boxes (Jiménez and Moin, 1991) that reduce the computational requirements. The present project also aims to provide estimates for ΔU^+ at a reduced cost, but removing the need to carry out turbulent simulations altogether, by capturing the effect of the geometry with a reduced order model, if possible.

In the present work we aim to gain insight into the physics triggering the transition from the hydraulically smooth regime. We carry out a series of direct numerical simulations (DNSs) of turbulent channels with rough walls. We study a roughness texture formed by equispaced square posts of the same size in a rectangular arrangement, as sketched in figure 2. Similar geometries have been studied by other authors (Leonardi et al., 2007; Leonardi and Castro, 2010) although their simulations mainly explore the fully rough regime. The purpose of our simulations is to investigate the evolution of turbulent flow fluctuations through the transitionally rough regime. The surface shape is kept constant throughout the simulations, but the size of the elements measured in wall units is varied from $k^+ \approx 6$ to $k^+ \approx 38$, aiming to span the whole transitionally rough regime. These flow fluctuations are split into turbulent and roughness-induced contributions. We restrict ourselves to the study of streamwise velocity fluctuations and leave the study of the other variables for future works. We aim to decompose the fluctuation into turbulent and roughness-induced contributions, with the purpose of isolating the effect of the roughness geometry.

The paper is organised as follows. In section 2 the numerical method is briefly described. We present statistics of the flow in section 3 and propose a decomposition of the flow in simpler components. Section 4 concludes this work.

2. The numerical method

The numerical experiments are conducted in a plane turbulent channel with rough texture on the top and bottom walls. The domain is periodic in the wall-parallel directions. The streamwise, wall-normal and spanwise coordinates are x, y and z, with u, v and w the corresponding components of the velocity $\boldsymbol{u}$. The flow is assumed incompressible with a density $\rho = 1$. The numerical method, briefly outlined below, is adapted from that of García-Mayoral and Jiménez (2011*b*) for riblet channels, is modified to handle fully three-dimensional geometries. The temporal integrator is a fractional-step method combined with a three-substep Runge-Kutta, and with pressure correction at the final step only (Le and Moin, 1991). The channel half-height is δ measured from the roughness tips, the length is $L_x = 2\pi\delta$ and the width $L_z = \pi\delta$. The spatial discretisation is pseudo-spectral. The two periodic directions, x and z, are discretised using Fourier series, while the wall-normal direction, y, is discretised using a second order finite difference scheme in a collocated grid. The integration of the pressure in these collocated grids commonly produces an undesired chequerboard effect (Ferziger and Perić, 2002). To avoid this issue, the code uses a quasi-divergence-free formulation based on the work by Nordström et al.

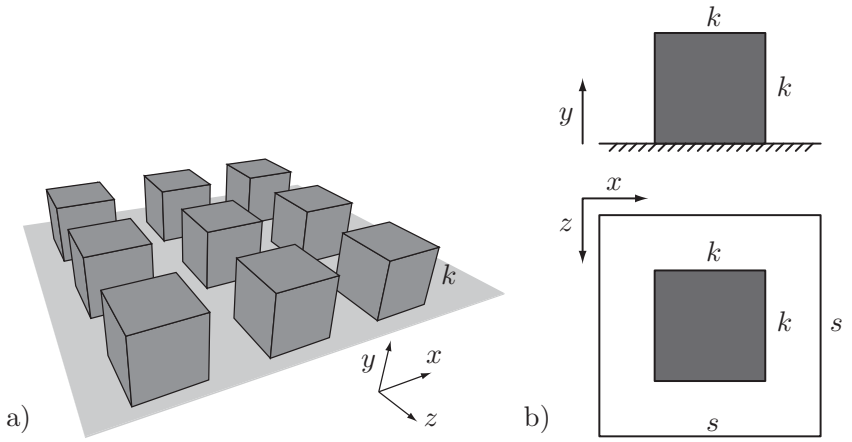

Figure 2. Sketch of the roughness geometry over the bottom wall. (a) Collocated arrangement of the elements. (b) Sketch of each periodic unit in the lattice shown in (a). In grey the post, formed by a cube of side k^+. The outer line represents the clearance between elements of size $s = 2k$.

(2007). This strategy consists of not enforcing exact incompressibility, $\nabla \cdot \boldsymbol{u} = 0$, and instead adding an evolution equation for $\nabla \cdot \boldsymbol{u}$ so that any divergence is rapidly damped. The grid in the y direction is non-uniform so that $\Delta y^+_{min} \approx 0.31$ at the wall and $\Delta y^+_{max} \approx 3.12$ at the centre of the channel. The domain is divided into three blocks in y with different x- and z-resolutions. This multi-block technique allows a high number of grid points to be set in the region near the walls, with a coarser resolution in the core of the channel. In this latter region the resolution is set to resolve all turbulent scales. In the blocks containing the walls it is also necessary to resolve the flow around the roughness elements as obstacles which requires a higher resolution for small k^+. The resolution in the central block is $\Delta^+_{x_c} \approx 6$ and $\Delta^+_{z_c} \approx 3$ in the x and z directions respectively, while in the other two blocks a finer resolution is used, $\Delta^+_{x_w} = \Delta^+_{z_w} \approx$ 1-2.

The simulations are run at constant flow rate, and the value of the viscosity is adjusted a priori for each simulation to keep the friction Reynolds number close to $\mathrm{Re}_\tau \approx 185$. Re_τ is computed using δ and the friction velocity u_τ obtained by extrapolating the total shear to an effective channel height δ'. This height is set so that $u_\tau^2 = -\delta' \partial p/\partial x$ (García-Mayoral and Jiménez, 2011*b*; Chung et al., 2015), which is the relationship that would hold for a smooth channel at δ. For the geometry under consideration this implies that δ' is measured from a virtual origin $y_0 = 1/8\, k$ below the roughness tips.

The roughness elements are introduced through a direct-forcing immersed boundary method (Mohd-Yusof, 1997; Fadlun et al., 2000; Iaccarino and Verzicco, 2003). The roughness geometry is depicted in figure 2. The unit element is a cube of side k, repeated along x and z in both walls with a texture period $s = 2k$.

3. Results

We conduct six DNSs with values of k^+ spanning the transitional regime. The parameters for the simulations are summarised in table 1.

Roughness is usually classified into k- and d-roughness. In k-roughness, the effective roughness k_s is proportional to k, while in d-roughness it is proportional to the boundary layer thickness (Jiménez, 2004). In the range of k^+ studied, our geometry displays conventional k-roughness behaviour, i.e. friction increases with k^+ and the mean velocity profile is shifted downwards, as shown in figure 3(a), increasing drag. In order to quantify this shift on the

Table 1. Parameters of the simulations. s^+ is the post spacing in both the streamwise and spanwise directions. The number of collocation points in the streamwise and spanwise directions are N_{x_c} and N_{z_c} in the middle block, and N_{x_w} and N_{z_w} in the top and bottom blocks. The resulting resolution is $\Delta^+_{x_w}$ and $\Delta^+_{z_w}$ in the middle block, and $\Delta^+_{x_c}$ and $\Delta^+_{z_c}$ in the top and bottom walls. N_y is the number of points in the y direction between roughness tips.

Case	k^+	s^+	ΔU^+	Re_τ	N_{x_c}	N_{z_c}	N_{x_w}	N_{z_w}	N_y
0C	–	–	–	184.5	192	192	192	192	153
6C	6.1	12.1	0.63	184.9	192	192	1152	576	153
9C	9.0	18.0	1.07	183.1	192	192	768	384	153
12C	12.0	24.0	1.90	183.6	192	192	1152	576	153
18C	17.8	35.5	3.81	181.0	192	192	768	384	153
24C	23.5	47.0	5.29	179.4	192	192	576	288	153
36C	37.9	75.8	7.37	193.0	192	192	768	384	153

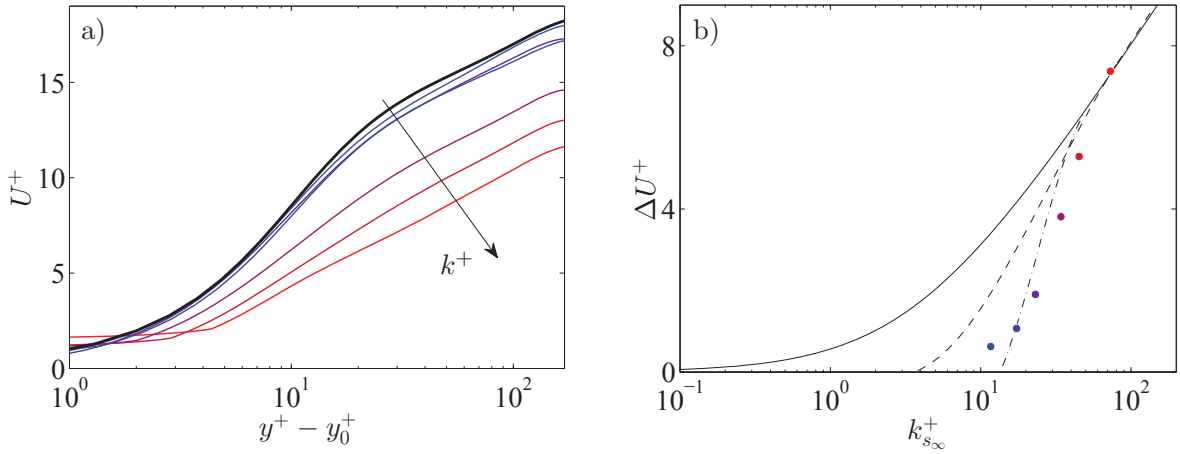

Figure 3. (a) Mean velocity profiles measured from $y_0^+ = 1/8\,k^+$. Thick black line, case 0C; blue to red, cases 6C through 36C of table 1. (b) Roughness function ΔU^+; —— , correlation for Colebrook results (Jiménez, 2004); – – – –, correlation of sand grain roughness (Nikuradse, 1933); –·– , correlation of sphere roughness (Ligrani and Moffat, 1986); ○ present DNSs using the same colors as in (a).

velocity profile and also be able to establish a comparison with other surfaces, we portray in figure 3(b) the roughness function, ΔU^+, against $k^+_{s_\infty}$, which for the geometry considered satisfies $k_{s_\infty}/k \approx 0.5$. This representation collapses the fully rough regime to a single asymptote, so the variations in the transitional regime for different surfaces can be compared. The roughness function of our cases is also compared to the results of Colebrook and White (1937), Nikuradse (1933), and Ligrani and Moffat (1986). In Colebrook and White (1937), Colebrook (1939), and Nikuradse (1933) the transition is smooth and begins at low values of $k^+_{s_\infty}$. In our case, the transitional regime resembles more closely that of the packed spheres of Ligrani and Moffat (1986), evolving rapidly from low to high values of ΔU^+. This is in agreement with the observation by Colebrook (1939) that regular roughness departs from the hydraulically smooth regime more gradually than regular roughness.

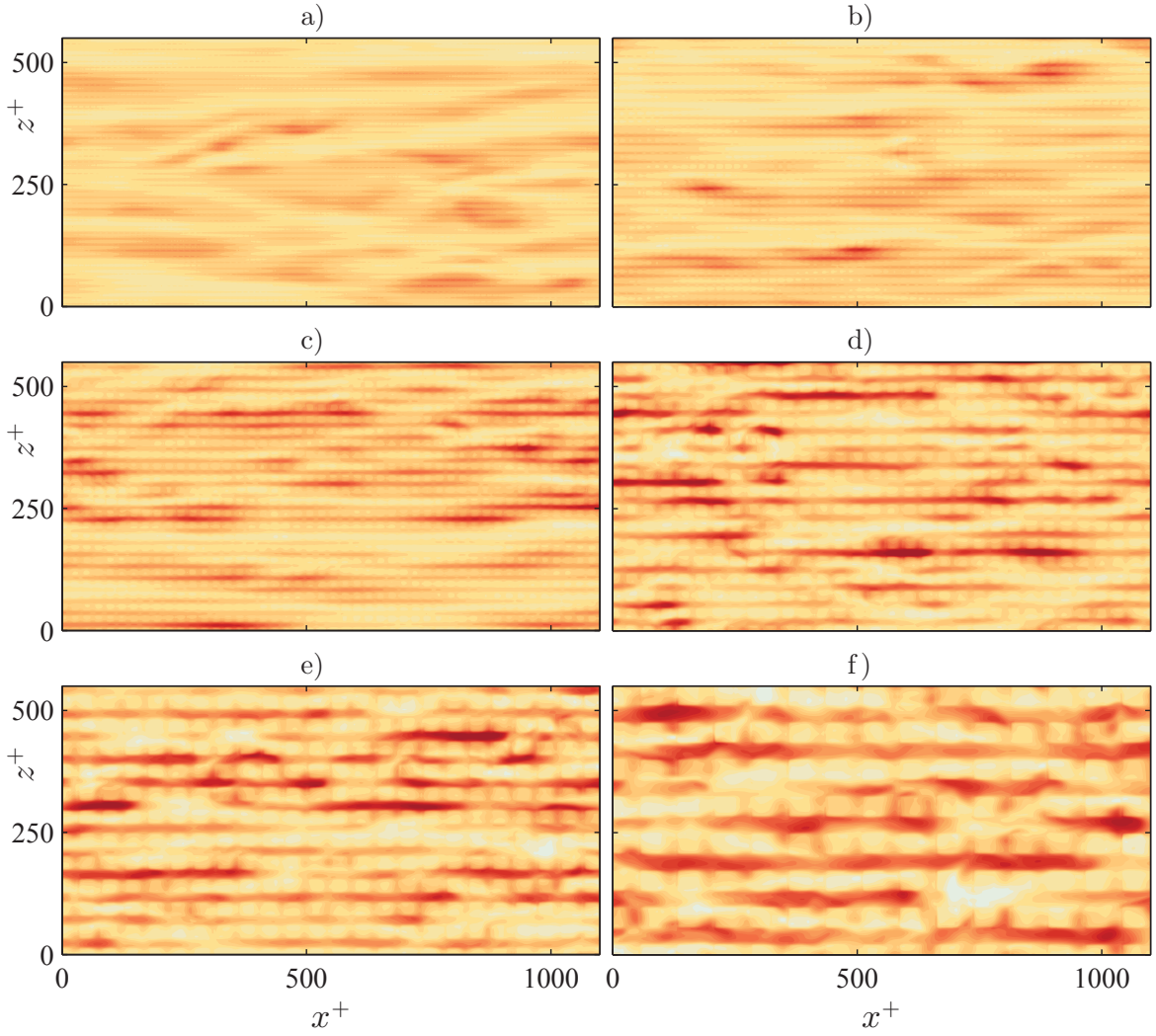

Figure 4. Instantaneous streamwise velocity at $y^+ \approx 1.3$ above roughness crest, for cases (a) 6C, (b) 9C, (c) 12C, (d) 18C, (e) 24C, and (f) 36C. The same scale of colour is used in all subfigures, with dark red and light yellow indicating high and low velocity, respectively.

3.1. Effect of roughness on the velocity fluctuations

To understand how the flow is modified by the presence of roughness, producing the changes in the mean flow described above, we focus our analysis on the velocity fluctuations. For the present paper, we restrict ourselves to the fluctuations of streamwise velocity. The analysis of the other velocity components and of the Reynolds stresses are left for future work.

The effect of roughness is limited to the vicinity of the wall, and decays rapidly away from it. As illustrating examples, figure 4 portrays instantaneous realizations of the streamwise velocity for cases 6C through 36C at $y^+ \approx 1.3$ above the roughness peaks, close enough to the wall to observe the effect of the roughness elements. The figure shows that the fluctuating velocity signal has two distinct contributions. The first is the typical background signal characteristic of wall turbulence, which consists of streamwise elongated streaks of high and low u-velocity, of length $500-1000$ wall units and width $50-100$ wall units (Kim et al., 1971; Smith and Metzler, 1983). This contribution remains essentially unmodified, at least for $k^+ < 15$ (or $\Delta U^+ < 3$). The second contribution is directly caused by the presence of the roughness elements, and consists of

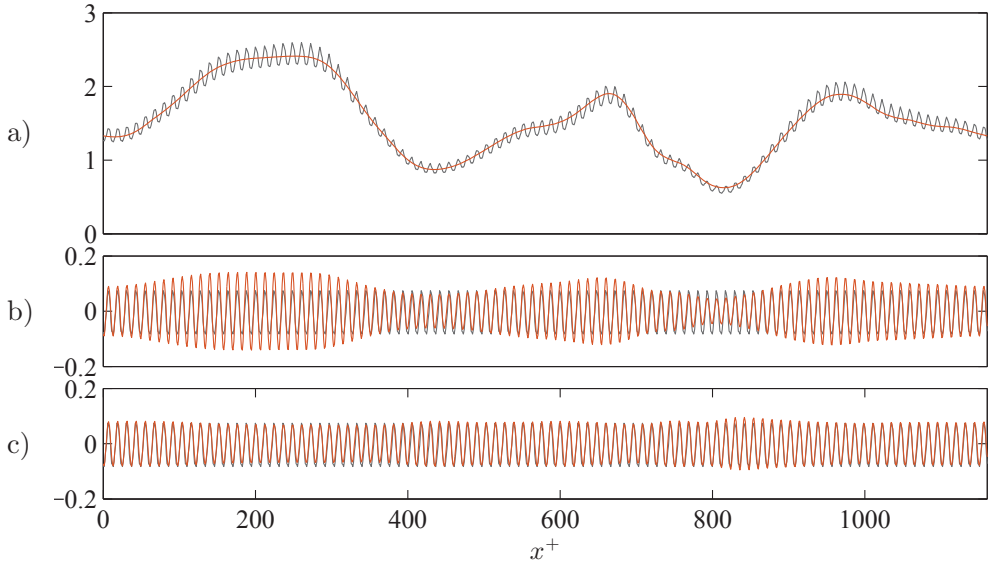

Figure 5. Instantaneous components of the streamwise velocity for case 12C at $y^+ \approx 0.7$ above roughness crest and a given z- section half-way between two rows of roughness elements. (a) In black, u; in red, u_T. (b) In black, $\overline{u}_R$; in red, u_R. (c) In black, $\overline{u}_R$ as obtained by averaging using equation 3; in red, $\overline{u}_R$ as obtained from equation 4.

alternating regions of relatively low velocity, right over the protruding elements, and relatively high velocities, over the valleys between elements. This signal is attached to the roughness geometry, and is therefore not advected over time as the turbulent contribution. It would instead be essentially repeated periodically in a lattice of streamwise and spanwise periodicity s, so that its value depends only on the relative position within each periodic unit, that is, the coordinates $\tilde{x}$ and $\tilde{z}$, with values between 0 and s, and the wall normal coordinate y. The lengthscales of this roughness contribution would scale with k^+, and its intensity would also increase with the roughness size.

To characterize these two contributions, we could try to decompose the flow as

$$u(x,y,z,t) = u_T(x,y,z,t) + \overline{u}_R(\tilde{x},y,\tilde{z}) = U(y) + u_S(x,y,z,t) + \overline{u}_R(\tilde{x},y,\tilde{z}), \tag{2}$$

where $\overline{u}_R$ would be the spatially fluctuating, time-independent component due to the roughness, and u_T the background turbulent signal, which would include the mean velocity $U(y)$ and the fluctuating component u_S, analogous to that over a smooth surface. The geometry-coherent signal $\overline{u}_R$ can be obtained by averaging over time and over the roughness lattice,

$$\overline{u}_R(\tilde{x},y,\tilde{z}) = |u(x,y,z,t) - U(y)|_{t,N_R}\,, \tag{3}$$

where N_R is the number of roughness elements in the simulation domain.

The above decomposition is analogous to that of Reynolds and Hussain (1972) for coherent waves in turbulence, and is widely used in flows over complex surfaces (Choi et al., 1993; Jiménez et al., 2001; García-Mayoral and Jiménez, 2011*b*; Jelly et al., 2014; Seo et al., 2015). However, the actual roughness-induced contribution, u_R, turns out to be different from the time-averaged $\overline{u}_R$, so we drop the decomposition of equation (2). The problem is illustrated in figure 5, which portrays the different contributions at a given instant and a given pair of coordinates z and y, that is, along an x-line, for case 12C. For this case k^+ is still small enough for the rough and turbulent components to have clearly separate wavelengths, so that u_T can be obtained

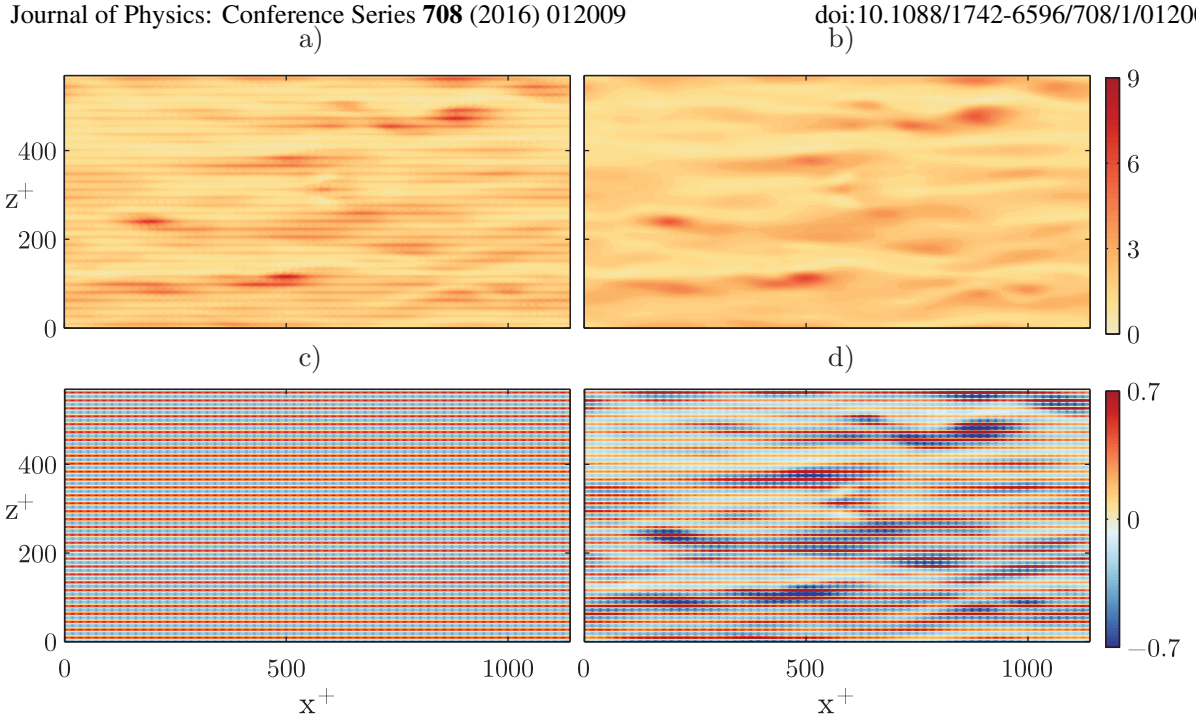

Figure 6. Instantaneous components of the streamwise velocity at $y^+ \approx 1.3$ above roughness crest for case 9C. (a) Full velocity signal u. (b) Background turbulent contribution u_T. (c) Coherent, time average signal induced by the presence of roughness, $\overline{u}_R$. (d) Instantaneous, u_T-modulated signal induced by the roughness, u_R.

simply by filtering out small wavelengths spectrally. Panel 5(a) shows the full velocity signal u superimposed with the filtered u_T, and illustrates the starting hypothesis that the velocity signal is made up of a turbulent signal, analogous to that over smooth walls, plus a small-intensity, small-wavelength, roughness-coherent signal. However, when u_T is subtracted from u, as portrayed in panel 5(b), the result is not exactly $\overline{u}_R$. The resulting u_R, is not exactly $\overline{u}_R$, but the modulation in amplitude of $\overline{u}_R$ by the turbulent u_T,

$$u_R = \frac{u_T}{U}\overline{u}_R. \tag{4}$$

Note that, on average, u_T/U is 1. Panel 5(c) shows how, once the modulation is removed from u_R, the coherent $\overline{u}_R$ is recovered.

Taking the above discussion into account, the correct decomposition that replaces equation (2) is

$$u = u_T + u_R = u_T + \frac{u_T}{U}\overline{u}_R, \tag{5}$$

which is essentially equation (2) with $\overline{u}_R$ replaced by u_R.

When both x and z are considered, the decomposition is a bit more complicated, but the discussion above serves to illustrate it. Furthermore, the spectral filtering only works when the wavelengths of u_T and $\overline{u}_R$ are clearly separated, which does not hold for the cases with larger k^+. However, it is always possible to obtain $\overline{u}_R$ by using equation (3) over the whole sampling history, and u_T can then be obtained algebraically from equation (5). The u_T-modulated, full roughness contribution, u_R, can be obtained once u_T and $\overline{u}_R$ are known using equation (4).

The result from decomposing the streamwise velocity using this procedure is shown for case 9C in figure 6. The comparison of panels (c) and (d), which portray respectively $\overline{u}_R$ and u_R, shows

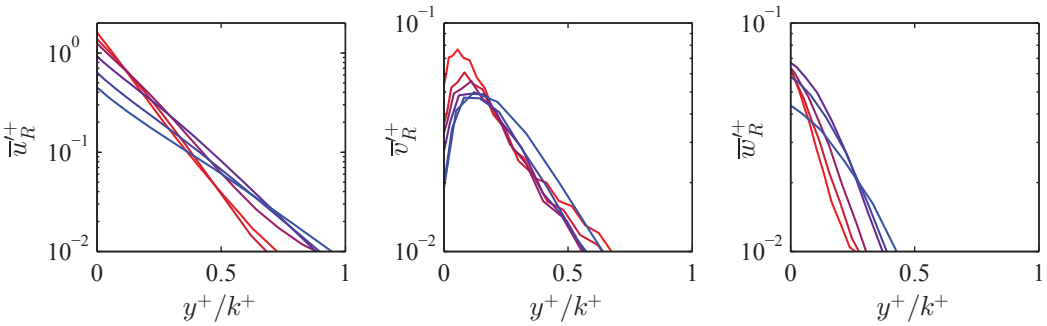

Figure 7. Root mean square of the coherent part of the velocity components. Blue to red, cases 6C through 36C.

how neglecting the amplitude modulation of u_R can lead to underpredicting its contribution to the total intensity of the fluctuations. Nevertheless, the perturbation caused by the surface on the flow decays rapidly away from the wall. Figure 7 shows the r.m.s. values, denoted by a 'prime' superscript, of the coherent part of the three velocity components, $\overline{u}_R$, $\overline{v}_R$ and $\overline{w}_R$. The three of them exhibit an exponential behaviour with a logarithmic slope roughly proportional to $-y/k$, which is to be expected from perturbations induced at the wall (Seo et al., 2015).

The present modulation of the near-wall, roughness-induced flow by the overlying turbulent flow is similar to the modulation of buffer-layer turbulence by outer-layer large structures, as presented by Marusic et al. (2010), except for the difference in the scales involved. In the present study, the modulating signal is actually the buffer-layer turbulence. The low Reynolds number of our DNSs prevents the development of large-scale turbulence, but if this was present it could be expected to modulate the buffer-layer flow. In turn, the total turbulent velocity above each roughness element would modulate the local u_R. This modulation of u_R by the overlying turbulence is also connected to the concept of protrusion height in riblets (Luchini et al., 1991; García-Mayoral and Jiménez, 2011*a*). For vanishing riblet spacing, the flow near each texture element is produced by the quasi-uniform shear induced by the turbulent eddy just above. In the scale of the texture, this eddy can be represented as quasi-infinite and quasi-steady. The overlying turbulent velocity therefore sets the scale for the local velocity within the riblet grooves, just like in our case the overlying u_T sets the scale for the local u_R.

The above discussion is only valid for vanishingly small roughness, when u_T modulates u_R but is itself unaffected by the presence of roughness. However, as the roughness size increases and becomes comparable to the turbulent eddies, this assumption ceases to hold. For the geometry considered in this paper, we would expect this to happen for $s^+ \approx 15-20$, when the spacing between roughness elements becomes comparable to the typical diameter of the quasi-streamwise vortices that are characteristic of near-wall turbulence (Kim et al., 1987). The validity of the assumption that u_T remains essentially unaffected by the presence of roughness can be checked in figure 8, which compiles the r.m.s. values of u^+, u_T^+ and u_R^+, denoted by a 'prime' superscript, as a function of y^+. Panel (c) shows how $u_R'^+$ increases gradually with k^+ from the smallest roughness, while significant changes in $u_T'^+$ only appear for $k^+ > 15$, or its equivalent roughness function $\Delta U^+ > 3$. This implies that the onset of roughness effects, that is, the beginning of the transitionally rough regime, can occur for roughness sizes at which the buffer-layer turbulence is essentially unaffected, so that it may be possible to estimate the changes in the flow independently of the turbulence.

This argument is further supported by the effect of the roughness under consideration on the r.m.s. of the streamwise vorticity $\omega_x'^+$, shown in figure 9. For the cases 6C, 9C and 12C,

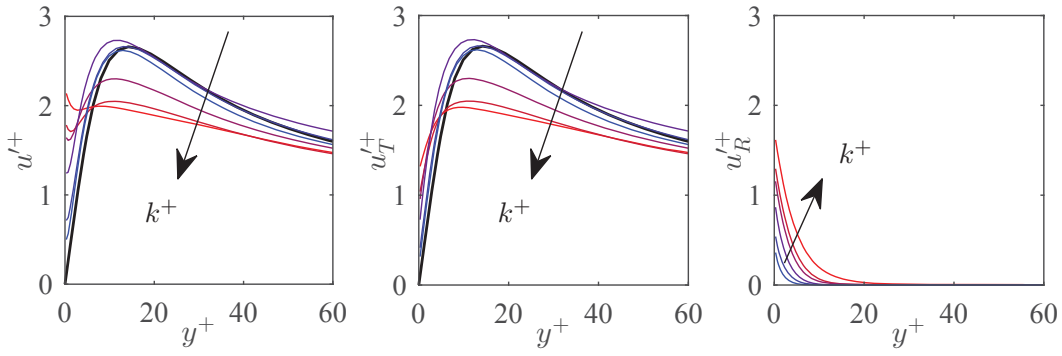

Figure 8. Root mean square of the different contributions to the streamwise velocity. From left to right, full u-signal, background-turbulence velocity u_T and roughness-induced velocity u_R. Thick black line, smooth channel (Hoyas and Jiménez, 2008); blue to red, cases 6C through 36C. The arrows indicate increasing k^+.

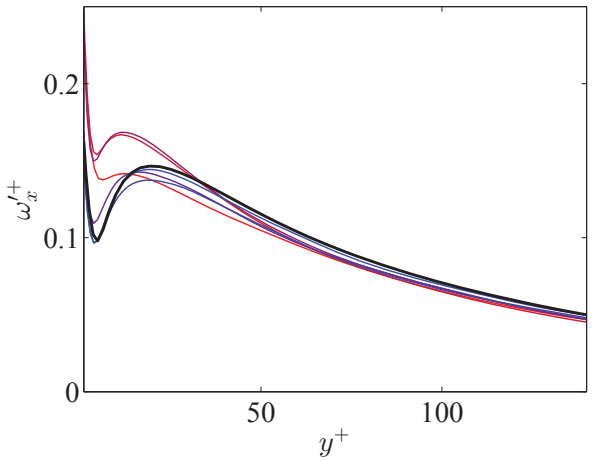

Figure 9. Root mean square of the streamwise vorticity with the origin of y placed at roughness crest. Lines coloured as in figure 8.

with $\Delta U^+ < 3$, the curves display no significant differences with that over a smooth wall, with similar values and the same distinctive maximum at $y^+ \approx 15$, which marks the average height of quasi-streamwise vortices. For slightly larger values of the roughness function, $\Delta U^+ \approx$ 4-6, the local maximum is shifted towards the wall and increases in magnitude. This may indicate an intensification and partial entrainment into the roughness troughs of the near-wall vortices, or a more complex interaction. Verifying this would require further studies, but in any event the change in the maximum marks a modification of the smooth-wall-like turbulence dynamics. For even larger roughness function, $\Delta U^+ > 7$, which is already in the fully rough range, the trend changes and the magnitude of the maximum decreases further, which could indicate a weakening of the quasi-streamwise vortices, and a more complete obliteration of the near-wall cycle by the roughness, as is typical of fully rough surfaces.

4. Conclusions and future work

We have focussed the present work in the transitionally rough regime of turbulent flows over rough walls. As a starting benchmark case, we have selected a surface made up of evenly spaced,

uniform cubes, and we have conducted a series of DNSs in which we have varied the size of the cubes, k^+, while maintaining the surface shape, so that the whole transitionally rough regime could be studied. We have hypothesised that the fluctuating flow could be decomposed into a smooth-wall-like turbulent contribution and a roughness-induced one. We have checked this assumption for the fluctuating streamwise velocity. For the small values of k^+ in the regime studied the decomposition is valid, except that the roughness-induced component is modulated in amplitude by the turbulent one. For somewhat larger k^+, the turbulent component differs from that over smooth walls, but in the onset of the transitionally rough regime the turbulent component remains essentially canonical, and all the changes in the flow can then be attributed to the geometry-induced component. This result suggests that it may be possible to predict the onset of roughness effects without considering the interaction of the roughness geometry with the turbulence, but further studies are required to verify this.

Acknowledgments
This work was supported by the European Research Council through the II Multiflow Summer Workshop, and by the British Engineering and Physical Sciences Research Council through grant number EP/M506485/1. We are grateful to Daniel Chung and Michael MacDonald for their careful critique of this manuscript.

References

Choi H, Moin P and Kim J 1993 Direct numerical simulation of turbulent flow over riblets *J. Fluid Mech.* **255**, 503–539.

Chung D, Chan L, MacDonald M, Hutchins N and Ooi A 2015 A fast direct numerical simulation method for characterising hydraulic roughness *J. Fluid Mech.* **773**, 418–431.

Colebrook C F 1939 Turbulent flow in pipes, with particular reference to the transitional region between smooth and rough wall laws *J. Inst. Civ. Eng.* **11**, 133–156.

Colebrook C F and White C M 1937 Experiments with fluid friction in roughened pipes *Proc. R. Soc. London Ser. A* **161**, 367–381.

Darcy H 1857 *Recherches expérimentales relatives au mouvement de l'eau*, Mallet-Bachelier Paris.

Fadlun E A, Verzicco R, Orlandi P and Mohd-Yusof J 2000 Combined immersed-boundary finite-difference methods for three-dimensional complex flow simulations *J. Comput. Phys.* **161**, 35–60.

Ferziger J H and Perić M 2002 *Computational methods for fluid dynamics* 3 edn Springer.

Flack K A and Schultz M P 2010 Review of hydraulic roughness scales in the fully rough regime *J. Fluids Eng.* **132**, 041203.

Flack K A and Schultz M P 2014 Roughness effects on wall-bounded turbulent flows *Phys. Fluids* **26**, 101305.

Flack K A, Schultz M P and Rose W B 2012 The onset of roughness effects in the transitionally rough regime *Int. J. Heat Fluid Flow* **35**, 160–167.

García-Mayoral R and Jiménez J 2011*a* Drag reduction by riblets. *Phil. Trans. R. Soc. A* **369**, 1412–1427.

García-Mayoral R and Jiménez J 2011*b* Hydrodynamic stability and breakdown of the viscous regime over riblets *J. Fluid Mech.* **678**, 317–347.

Hama F R 1954 Boundary-layer characteristics for smooth and rough surfaces *Trans. Soc. Naval Archit. Mar. Eng.* **62**, 333–358

Hoyas S and Jiménez J 2008 Reynolds number effects on the Reynolds-stress budgets in turbulent channels *Phys. Fluids* **20**, 101511.

Iaccarino G and Verzicco R 2003 Immersed boundary technique for turbulent flow simulations *Appl. Mech. Rev.* **56**, 331–347.

Jelly T O, Jung S Y and Zaki T A 2014 Turbulence and skin friction modification in channel flow with streamwise-aligned superhydrophobic surface texture *Phys. Fluids* **26**, 095102.

Jiménez J 2004 Turbulent flows over rough walls *Annu. Rev. Fluid Mech.* **36**, 173–196.

Jiménez J and Moin P 1991 The minimal flow unit in near-wall turbulence *J. Fluid Mech.* **225**, 213–240.

Jiménez J, Uhlmann M, Pinelli A and Kawahara G 2001 Turbulent shear flow over active and passive porous surfaces *J. Fluid Mech.* **442**, 89–117.

Kim H T, Kline S J and Reynolds W C 1971 The production of turbulence near a smooth wall in a turbulent boundary layer *J. Fluid Mech.* **50**, 133–160.

Kim J, Moin P and Moser R D 1987 Turbulence statistics in fully developed channel flow at low Reynolds number *J. Fluid Mech.* **177**, 133–166.

Le H and Moin P 1991 An improvement of fractional step methods for the incompressible Navier-Stokes equations *J. Comput. Phys.* **92**, 369–379.

Leonardi S and Castro I P 2010 Channel flow over large cube roughness: a direct numerical simulation study *J. Fluid Mech.* **651**, 519.

Leonardi S, Orlandi P and Antonia R A 2007 Properties of d- and k-type roughness in a turbulent channel flow *Phys. Fluids* **12**, 125101.

Ligrani P M and Moffat R J 1986 Structure of transitionally rough and fully rough turbulent boundary layers *J. Fluid Mech.* **162**, 69–98.

Luchini P, Manzo F and Pozzi A 1991 Resistance of a grooved surface to parallel flow and cross-flow *J. Fluid Mech.* **228**, 87–109.

Marusic I, Mathis R and Hutchins N 2010 Predictive model for wall-bounded turbulent flow. *Science* **329**, 193–196.

Mohd-Yusof J 1997 Combined immersed-boundary/B-spline methods for simulations of flow in complex geometries *Annu. Res. Briefs Center Turbul. Res.* pp. 317–327, Stanford Univ.

Nikuradse J 1933 Laws of flow in rough pipes *VDI-Forsch.* **361**

Nordström J, Mattsson K and Swanson C 2007 Boundary conditions for a divergence free velocity-pressure formulation of the Navier–Stokes equations *J. Comput. Phys.* **225**, 874–890.

Raupach M R, Antonia R A and Rajagopalan S S 1991 Rough-wall turbulent boundary layers *Appl. Mech. Rev.* **44**, 1–25.

Reynolds W C and Hussain A K M F 1972 The mechanics of an organized wave in turbulent shear flow. Part 3. Theoretical models and comparisons with experiments *J. Fluid Mech.* **54**, 263–288.

Schlichting H 1936 Experimental investigation of the problem of surface roughness *NACA Tech. Memo* 823.

Schultz M P and Flack K A 2007 The rough-wall turbulent boundary layer from the hydraulically smooth to the fully rough regime *J. Fluid Mech.* **580**, 381–405.

Seo J, García-Mayoral R and Mani A 2015 Pressure fluctuations in turbulent flows over superhydrophobic surfaces *J. Fluid Mech.* **783**, 448–473.

Smith C and Metzler S 1983 Characterization of low-speed streaks in the near-wall region of a turbulent boundary layer *J. Fluid Mech.* **129**, 27–54.